Inorg. Chem. **2007**, *46*, 2208–2219

Iron Complexes of New Pentadentate Ligands Containing the 1,4,7-Triazacyclononane-1,4-diacetate Motif. Spectroscopic, Electro-, and Photochemical Studies

Yu-Fei Song,*[,†,‡] John F. Berry,*[,†,||] Eckhard Bill,[†] Eberhard Bothe,[†] Thomas Weyhermüller,[†] and Karl Wieghardt[†]

Max-Planck-Institut für Bioanorganische Chemie, Stiftstrasse 34-36, D-45470 Mülheim an der Ruhr, Germany, and Department of Chemistry, University of Wisconsin, 1101 University Avenue, Madison, Wisconsin 53706

Received October 19, 2006

Three new pentadentate, pendent arm macrocycles containing the 1,4,7-triazacyclononane-1,4-diacetate motif have been synthesized, and their coordination chemistry with Fe(III) has been investigated. Eight new octahedral Fe(III) complexes containing chloro, azido, or μ-oxo ligands have been synthesized, five of which have been characterized by X-ray crystallography. Spectroscopic characterization of these octahedral Fe(III) complexes by UV–vis, IR, electrochemistry, EPR, magnetic susceptibility, and zero-field Mössbauer measurements firmly establishes the high-spin state of the iron in all complexes. Electrochemistry studies of the azido–Fe(III) complexes show that they can be reversibly oxidized to the corresponding Fe(IV) species at –20 °C, and Fe(II), Fe(III), and Fe(IV) species show characteristic IR and UV–vis profiles. Photolysis of one of the azido complexes was studied as a function of temperature (room temperature vs 77 K) and wavelength (480, 419, and 330 nm). Photoreduction to a high-spin Fe(II) species occurs under all conditions, which is proposed to be the dominant photochemical pathway generally available to high-spin ferric azido complexes.

Introduction

1,4,7-Triazacyclononane (TACN) is now a classical ligand in inorganic chemistry; it and many *N*-functionalized derivatives have been applied in several different areas of chemistry for many years.[1−3] The TACN ring binds metals strongly to cover a trigonal face of an octahedrally coordinated transition metal ion, providing kinetic stability to the complex and useful control over the remaining environment. In addition, TACN is a pure σ-donor and is therefore "innocent" in a spectroscopic sense, as well as a redox sense, meaning that all redox processes exhibited by TACN complexes may safely be assumed to be metal-based. This distinguishes TACN and other saturated macrocycles such as 1,4,8,11-tetraazacyclotetradecane[4] (cyclam) from conjugated macrocyclic ligands such as porphyrins[5] or corroles.[6]

Pentadentate pendent arm derivatives of TACN are currently of interest because these macrocycles can be utilized to construct mononuclear octahedral complexes that possess a single open coordination site allowing the binding and activation of small molecules.[3,7−9] Such systems are nevertheless rare compared with hexadentate *N*,*N*′,*N*″-trifunctionalized TACN ligand systems and their chelate complexes.[1] The majority of reported complexes with pentadentate derivatives of TACN and related macrocycles are complexes

* To whom correpondence should be addressed. E-mail: ysong@chem.gla.ac.uk (Y.-F.S.); berry@chem.wisc.edu (J.F.B.).

† Max-Planck-Institut für Bioanorganische Chemie.

‡ Current Address: Department of Chemistry, University of Glasgow, G12, 8QQ, Glasgow, UK.

|| University of Wisconsin—Madison.

(1) Chaudhuri, P.; Wieghardt, K. *Prog. Inorg. Chem.* **1987**, *35*, 329.
(2) Bernhardt, P. V.; Lawrance, G. A. *Coord. Chem. Rev.* **1990**, *104*, 297.
(3) Lindoy, L. F. *The Chemistry of Macrocyclic Ligands*; Cambridge University Press: Cambridge, 1989.
(4) Bosnich, B.; Poon, C. K.; Tobe, M. L. *Inorg. Chem.* **1965**, *4*, 1102.
(5) Rutter, R.; Hager, L. P.; Dhonau, H.; Hendrich, M.; Valentine, M.; Debrunner, P. *Biochemistry* **1984**, *23*, 6809.
(6) (a) Nardis, S.; Paolesse, R.; Licoccia, S.; Fronczek, F. R.; Vicente, M. G. H.; Shokhireva, T. K.; Cai, S.; Walker, F. A. *Inorg. Chem.* **2005**, *44*, 7030. (b) Walker, F. A.; Licoccia, S.; Paolesse, R. *J. Inorg. Biochem.* **2006**, *100*, 810. (c) Gross, Z.; Gray, H. B. *Comments Inorg. Chem.* **2006**, *27*, 61.
(7) Warden, A. C.; Spiccia, L.; Hearn, M. T. W.; Boas, J. F.; Pilbrow, J. R. *Dalton Trans.* **2005**, 1804.
(8) McAuley, A.; Subramanian, S.; Zaworotko, M. J.; Atencio, R. *Inorg. Chem.* **1998**, *37*, 4607.
(9) Fallon, G. D.; McLachlan, G. A.; Moubaraki, B.; Murray, K. S.; O'Brien, L.; Spiccia, L. *J. Chem. Soc., Dalton Trans.* **1997**, 2765.

10.1021/ic062001j CCC: $37.00
Published on Web 02/22/2007

Scheme 1

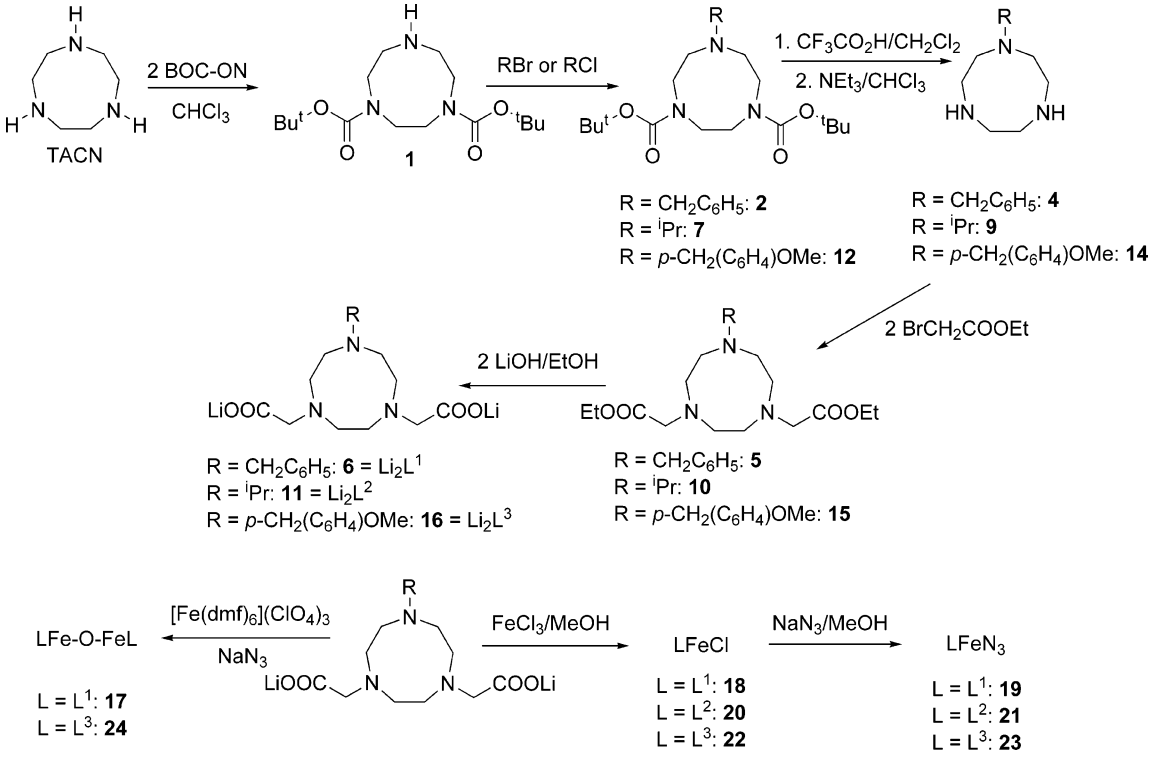

of Cu(II),[7] Mn(II),[9] and Cr(III),[9] though Fe(III) complexes with pentadentate TACN-derived ligands having pendent pyridyl arms are known.[9] Therefore, we have investigated the coordination chemistry of three new pentadentate ligands containing the 1,4,7-triazacyclononane-1,4-diacetate motif and their resulting iron complexes. This work was instigated by recent advances in the chemistry of iron in oxidation states higher than +3. In particular, the discovery that ferric azido cyclam complexes[10] and later, azido cyclam−acetate complexes[11] undergo photo-oxidation to yield unstable Fe(V)−nitrido species was important. By changing the macrocyclic ligand from a mono-pendent arm cyclam−acetate to the bis-pendent arm TACN−diacetate, two important changes are made. First, the charge of the ligand is increased from 1− to 2−, which should better stabilize the positive charge of higher-valent iron ions. Also, the symmetry of the resulting iron complexes is dramatically changed: iron cyclam complexes having two more ligands trans to each other are tetragonally distorted leading to a splitting in the t_{2g} orbitals such that the d_{xy} orbital lies significantly lower in energy than the nearly degenerate d_{xz}, d_{yz} pair. TACN-based complexes are often trigonally distorted, which causes a much larger splitting between the d_{xz} and d_{yz} orbitals. This is desirable because the known tetragonal Fe(V)−nitrido complexes possess a nearly orbitally degenerate $S = 1/2$ ground state due to the presence of one unpaired electron in the d_{xz}, d_{yz} set.[12] In order to judge the effects of orbital degeneracy of the Fe(V) system on its reactivity, we were intensely interested in the photolysis products of the trigonally distorted Fe(III) complexes reported herein.

In this paper, three new pentadentate ligands (Scheme 1) containing the 1,4,7-triazacyclononane-1,4-diacetate motif and eight new octahedral Fe(III) complexes containing chloro, azido, or μ-oxo ligands have been prepared and characterized. The spectroscopic, electro-, and photochemical studies of these azido−Fe(III) compounds are presented, and although no evidence for photo-oxidation to Fe(V) has been obtained for these complexes, some very interesting Fe(IV) species have been electrochemically generated and studied.

Experimental Section

Caution: *Although we have not encountered any problems, it should be kept in mind that perchlorate salts and metal azides are potentially explosive and should be handled carefully only in small amounts with appropriate precautions.*

The solvents diethyl ether, toluene, ethanol, dichloromethane, chloroform, methanol, acetonitrile, *n*-hexane, and *n*-pentane were commercially available and dried over molecular sieves before use; triethylamine was dried over Na_2SO_4 overnight. The chemicals bromoacetic acid ethyl ester, 2-*tert*-butoxycarbonyloxyimino-2-phenylacetonitrile (BOC-ON), trifluoroacetic acid, citric acid, iron powder, 1-chloromethyl-4-methoxybenzene, sodium metal, $NaBH_4$, NaOH, KOH, K_2CO_3, acetone, 2-propanol, and dimethylformamide (DMF) were obtained from commercial sources and used without further purification.

TACN was synthesized as described in the literature.[13] $[Fe(dmf)_6](ClO_4)_3$ was synthesized by refluxing $Fe(ClO_4)_3$ in dry DMF for several hours, and the compound was obtained as a yellow

(10) Meyer, K.; Bill, E.; Mienert, B.; Weyhermüller, T.; Wieghardt, K. *J. Am. Chem. Soc.* **1999**, *121*, 4859.
(11) Grapperhaus, C. A.; Mienert, B.; Bill, E.; Weyhermüller, T.; Wieghardt, K. *Inorg. Chem.* **2000**, *39*, 5306.
(12) Aliaga-Alcalde, N.; DeBeer George, S.; Mienert, B.; Bill, E.; Wieghardt, K.; Neese, F. *Angew. Chem., Int. Ed.* **2005**, *44*, 2908.
(13) Wieghardt, K.; Schmidt, W.; Nuber, B.; Weiss, J. *Chem. Ber.-Recl.* **1979**, *112*, 2220.

precipitate. This starting material was characterized by satisfactory C, H, N, Fe, and Cl elemental analysis.

Synthesis of Li_2L1 (R = Benzyl). 1,4,7-Triazacyclononane-1,4-dicarboxylic acid di-*tert*-butyl ester **(1)** was synthesized according to the literature.[14] Yield: 66%. ^{1}H NMR (400 MHz, chloroform-*d*): 1.42 (s, 18H, *t*-Bu), 2.87 (m, 4H, TACN ring), 3.19 (m, 4H, TACN ring), 3.40 (m, 4H, TACN ring). ESI-MS spectrometry (positive mode, MeOH) m/z = 329 (M^+). Anal. Calcd for $C_{16}H_{31}N_3O_4$ (329.4 g/mol): C 58.33, H 9.48, N, 12.76; Found: C 58.62, H 9.86, N 12.24.

7-Benzyl-1,4,7-triazacyclononane-1,4-dicarboxylic Acid Di-*tert*-butyl Ester (2). KOH (2.63 g, 46.9 mmol) was added to a solution of compound **1** (4.67 g, 14.2 mmol) in toluene (50 mL) at room temperature. To this mixture was added benzyl bromide (2.91 g, 17.0 mmol) in toluene (20 mL) within 10 min. The reaction mixture was kept stirring at 70 °C for 24 h, during which the reaction was monitored by TLC until the starting material **(1)** reacted completely. Then, the reaction mixture was filtered, dried over $MgSO_4$, and concentrated under reduced pressure to give **2** as yellow oil. Yield: 5.6 g, 95%. ^{1}H NMR (400 MHz, chloroform-*d*): 1.43 (s, 9H, *t*-Bu), 1.49 (s, 9H, *t*-Bu), 2.34 (s, 2H, $-CH_2-$), 3.14 (m, 4H, TACN ring), 3.21 (m, 4H, TACN ring), 3.51 (m, 4H, TACN ring), 7.14 (m, 2H, −benzene ring), 7.16 (t, 1H, J = 7.0 Hz), 7.32 (m, 2H, −benzene). ESI-MS spectrometry (positive mode, MeOH) m/z = 420 (M^+).

4-Benzyl-1,4,7-triazacyclononane-1,4,7-ium Bis(trifluoroacetate) (3). To a solution of **2** (8.0 g, 19.0 mmol) in CH_2Cl_2 (20 mL) was added 50% CF_3CO_2H/CH_2Cl_2 (100 mL) at 0 °C. The solution was stirred at 0 °C for 2.5 h, during which the reaction was examined by TLC. Then, the solution was concentrated under reduced pressure and diethyl ether was added to the obtained residue. The solvent was removed by rotary evaporation in order to remove the excess CF_3CO_2H, and this process was repeated three times. A light yellow powder was obtained, which was washed with Et_2O/*n*-hexane (1:1, 200 mL) several times and dried under vacuum. Yield: 8.7 g, 82%. ESI mass spectrometry (positive mode, MeOH) indicated CF_3CO_2H free fragment. m/z = 220 $(M' + H)^+$. ^{1}H NMR (400 MHz, CD_3OD-d_4): 3.05 (br, 4H, TACN ring), 3.46 (br, 4H, TACN ring), 3.60 (s, 2H, $-CH_2-$), 3.80 (br, 4H, TACN ring), 7.31 (m, 5H, −benzene ring).

1-Benzyl-1,4,7-triazacyclononane (4). To a cold (0 °C) solution of **3** (8.0 g, 14.2 mmol) in $CHCl_3$ (120 mL) was added Et_3N (10 mL). The solution was stirred at 0 °C for 1 h and then washed with saturated NaCl solution (3 × 300 mL). The organic phase was dried over $MgSO_4$ and concentrated under reduced pressure to give **4** as a yellow oil. Yield: 2.8 g, 90%. ^{1}H NMR (400 MHz, chloroform-*d*): 2.10, (br, 2H, TACN ring), 2.62 (m, 6H, TACN ring), 2.75 (m, 4H, TACN ring), 3.68 (s, 2H, $-CH_2-$), 7.22 (m, 5H, −benzene ring). ESI-MS spectrometry (positive mode, MeOH) m/z = 220 $(MH)^+$.

4-Benzyl-7-ethoxycarbonylmethyl-1,4,7-triazacyclononane-1-yl Acetic Acid Ethyl Ester (5). To a solution of **4** (3.6 g, 16.4 mmol) in EtOH (30 mL) was added bromoacetic acid ethyl ester (5.62 g, 33.8 mmol) at room temperature. Then, the solution was cooled to 0 °C and to this was added sodium metal (0.78 g, 33.8 mmol) dissolved in EtOH (40 mL). The solution was kept stirring at 0 °C for 1 h, during which the reaction was examined by TLC until the starting material **4** reacted completely. Then, the solution was concentrated under reduced pressure. To the obtained residue was added 50 mL of toluene, and the mixture was stirred for 2 h in order to precipitate NaBr. The solution was filtered and the filtrate was concentrated under reduced pressure to give a yellow oil, which was extracted with Et_2O/*n*-hexane (1:1, 250 mL). The organic phase was concentrated under reduced pressure, and the residue was dried under vacuum to give a yellow oil. Yield: 3.8 g, 65%. ^{1}H NMR (400 MHz, chloroform-*d*): 1.28 (m, 6H, $-CH_3$), 2.91 (m, 12H, TACN ring), 3.34 (d, 2H, $-CH_2-COO-$, J = 16.3 Hz), 3.40 (d, 2H, $-CH_2-COO-$, J = 16.3 Hz), 3.68 (s, 2H, $-CH_2-$), 4.13 (m, 4H, $-CH_2-CH_3$), 7.30 (m, 5H, −benzene ring). ESI-MS spectrometry (positive mode, MeOH) m/z = 391 (M^+).

4-Carboxymethyl-7-benzyl-1,4,7-triazacyclononan-1-yl Acetic Acid Lithium Salt (6). To a solution of **5** (5.4 g, 13.8 mmol) in EtOH (50 mL) was added finely powdered $LiOH\cdot H_2O$ (1.26 g, 30 mmol). The mixture was refluxed at 70 °C for 24 h and then filtered; the filtrate was concentrated under reduced pressure to give a pale yellow solid. The solid was washed with cold ethanol, Et_2O, and dried under vacuum. Yield: 3.6 g, 70%. ^{1}H NMR (400 MHz, CD_3-OD-d_4): δ 2.27 (m, 2H, TACN ring)), 2.56 (m, 4H, TACN ring), 2.73 (m, 6H, TACN ring), 3.12 (d, 2H, $-CH_2-$, J = 16.4 *Hz*), 3.26 (d, 2H, -CH_2-, J = 16.4 *Hz*), 3.80 (s, 2H, $-CH_2-$), 7.29 (t, 1H J = 7.2 Hz), 7.37 (t, 2H, J = 7.4 Hz), 7.45 (d, 2H, J = 7.2 Hz). ^{13}C NMR (100 MHz, CD_3OD-d_4): δ 52.83 ($-CH_2-$), 54.16 ($-CH_2-$), 54.54 ($-CH_2-$), 63.34 ($-CH_2-$), 64.07 ($-CH_2-$), 129.08 ($-CH-$), 129.90 ($-CH-$), 132.03 ($-CH-$), 138.52 ($-C-$), 181.31 ($-CO_2-$). ESI-MS spectrometry (negative mode, MeOH) m/z = 334 ($[Li_2L1 - 2Li + H]^-$). Anal. Calcd for $Li_2L1\cdot 2LiOH\cdot H_2O$ ($C_{17}H_{27}N_3O_7Li_4$, 413.2 g/mol); C 49.42, H 6.59, N 10.17; Found C 49.82, H 6.48, N 9.97. IR (KBr, cm^{-1}): 3412 (b), 1590(b), 1494 (w), 1441 (m), 1411 (s), 1331 (m), 1120 (s), 1101 (m), 1078 (m), 1050 (w), 1003 (m), 928(w), 899 (w), 728 (m), 705 (m), 635 (w), 487 (w).

Syntheses of Li_2L2 and Li_3L3 were carried out in a similar way to that of Li_2L1, and the detailed synthetic procedures can be found in the Supporting Information.

Preparation of Complexes. 2[L1Fe(μ-O)FeL1]·$NaPF_6$·$14H_2O$·3MeOH (17). A solution of **6** (120 mg, 0.29 mmol) in MeOH (10 mL) was added to $Fe(dmf)_6(ClO_4)_3$ (254 mg, 0.29 mmol) in MeOH (10 mL). The reaction mixture was refluxed for 1.5 h, and a yellow solution with a yellow precipitate was formed. Then, NaN_3 (188.5 mg, 2.9 mmol) in MeOH (10 mL) was added to the solution and a clear, red solution formed immediately. The solution was allowed to stir for 1.5 h, and then a saturated aqueous solution of KPF_6 (5 mL) was added. The resulting solution was concentrated to 10 mL and filtered; diffusion of diethyl ether into the filtrate resulted in the formation of red square-shaped crystals. Yield: 203 mg, 67%. Anal. Calcd for the complex [L1Fe(μ-O)FeL1]·$0.5NaPF_6$·$7H_2O$·1.5MeOH ($C_{35.5}H_{61}F_3Fe_2N_6Na_{0.5}O_{17.5}P_{0.5}$, 1047.59 g/mol) C 40.70, H 5.82, N 8.02; Found C 41.13, H 5.34, N 8.22. ESI-MS spectrometry (positive mode, MeOH) m/z = 833 ([L1-Fe-O-Fe-L1 + K]$^+$). IR (KBr, cm^{-1}): 3446(s), 1635 (s, C═O), 1496 (w), 1458 (m), 1358 (s), 1314 (w), 1099 (s), 1007 (w), 967 (w), 927 (m), 846 (s), 806 (s), 773 (m), 725 (w), 626 (m), 561 (m). It should be mentioned here that this compound can also be obtained by using $FeCl_3\cdot 6H_2O$ instead of $Fe(dmf)_6(ClO_4)_3$.

[L1-Fe-Cl]·0.5EtOH·0.5H_2O (18). Compound **6** (240 mg, 0.58 mmol) was added to $FeCl_3$ (97 mg, 0.58 mmol) in MeOH (20 mL). The reaction mixture was refluxed for 2 h, and then the resulting yellow precipitate was collected by filtration and dried at room temperature. Recrystallization of the compound from EtOH/H_2O (1:1, 30 mL) resulted in the formation of yellow crystals suitable for X-ray crystallographic analysis after 1 week. Yield: 187 mg, 70%. Anal. Calcd for L1-Fe-Cl·$0.5EtOH\cdot 0.5H_2O$ ($C_{18}H_{27}N_3O_5FeCl$, 456.7 g/mol) C 47.34, H 5.96, N 9.20; Found C 47.52, H 6.31, N

(14) Kimura, S.; Bill, E.; Bothe, E.; Weyhermüller, T.; Wieghardt, K. *J. Am. Chem. Soc.* **2001**, *123*, 6025.

8.95. ESI-MS spectrometry (positive mode, MeOH) $m/z = 389$ ($[L1 - Fe]^+$ 100%), 424 ($[L1 - Fe - Cl]^+$ 60%). IR (KBr, cm^{-1}): 3539 (s), 1665 (s, C═O), 1488 (m), 1461 (m), 1451 (m), 1346 (s), 1328 (s), 1315 (s), 1279 (s), 1251 (w), 1228 (w), 1094 (m), 1079 (m), 1065 (m), 1040 (m), 1022 1010, 967 (s), 922 (s), 839 (m), 812 (m), 762 (s), 729 (m), 704 (s), 652(s), 562 (m), 507 (m), 487 (m), 455 (w), 421(w).

[L1-Fe-N_3] (19). Compound **18** (77.5 mg, 0.17 mmol) was dissolved in MeOH (20 mL), to which NaN_3 (11 mg, 0.17 mmol) was then added. The reaction mixture was stirred at room temperature for 3 h, and a red solid precipitated. The solution was filtrated, and the solid was recrystallized from MeCN/MeOH (6:4, 30 mL) in the dark. Orange, needle crystals were formed after 1 week, which were suitable for X-ray crystallography. Yield: 48 mg, 66%. Anal. Calcd for the complex [L1-Fe-N_3] ($C_{17}H_{23}N_6O_4$-Fe, 431.2 g/mol) C 47.35, H 5.38, N 19.49; Found C 46.98, H 5.24, N 19.23. ESI-MS spectrometry (positive mode, MeOH) $m/z = 431$ ($[L1\text{-Fe-}N_3]^+$). IR (KBr, cm^{-1}): 3463 (s), 2066 (s, N_3), 1676 (s, C═O), 1492 (w), 1320 (m), 1283 (s), 1089 (w), 1064 (w), 914 (s), 812 (m), 771 (m), 712 (s), 559 (w).

[L2-Fe-Cl]·0.5MeOH (20). A solution of **11** (274 mg, 0.66 mmol) in MeOH (10 mL) was added to $FeCl_3$ (106 mg, 0.66 mmol) in MeOH (10 mL). The reaction mixture was heated to reflux for 2 h, and the resulting yellow precipitate was filtered and dried under vacuum. Recrystallization of the compound from MeOH/H_2O (7:3, 50 mL) led to the formation of yellow crystals after 1 week. Yield: 194 mg, 75%. Anal. Calcd for L2-Fe-Cl·0.5MeOH ($C_{13.5}H_{25}N_3O_{4.5}$FeCl, 392.4 g/mol) C 41.32, H 6.37, N 10.70; Found C 41.54, H 6.82, N 10.43. ESI-MS spectrometry (positive mode, MeOH) $m/z = 341$ ($[L2\text{-Fe}]^+$ 100%) and 377 ($[L2\text{-Fe-Cl}]^+$ 70%). IR (KBr, cm^{-1}): 3421 (m), 1671 (s, C═O), 1492 (m), 1459 (m), 1331 (s), 1293 (s), 1093 (m), 1030 (w), 1004 (w), 922 (m), 823 (m), 714(m).

[L2-Fe-N_3] (21). This compound was synthesized by reaction of 1 equiv each of compound **20** and NaN_3 in MeOH. The reaction mixture was stirred for 3 h, and small amount of precipitate was removed by filtration. The filtrate was allowed to evaporate at room temperature in the dark. Orange crystals suitable for X-ray crystallography formed after 1 week. Yield: ~52%. Anal. Calcd for the complex L2-Fe-N_3 ($C_{13}H_{23}N_6O_4$Fe, 383.2 g/mol) C 40.75, H 6.05, N 21.93; Found C 40.28, H 6.23, N 21.38. ESI-MS spectrometry (positive mode, MeOH) $m/z = 383$ ($[L2\text{-Fe-}N_3]^+$). IR (KBr, cm^{-1}): 3431 (m), 2964 (w), 2066 (s, N_3), 1674 (s, C═O), 1497 (w), 1460 (w), 1335 (s), 1296 (s), 1278 (s), 1090 (w), 1078 (m), 1027 (m), 924 (s) 811 (m), 720 (m), 620 (w), 562 (w), 491 (w), 470 (m), 415 (w)

[L3-Fe-Cl·H_2O] (22). A solution of **16** (365 mg, 0.66 mmol) in MeOH (10 mL) was slowly added to a solution of $FeCl_3$ (107.5 mg, 0.66 mmol) in MeOH (10 mL). The reaction mixture was refluxed for 2 h and filtered. The filtrate was kept at room temperature, and yellow crystals were obtained after 3 weeks. Yield: 218 mg, 70%. Anal. Calcd for the complex L3-Fe-Cl·H_2O ($C_{18}H_{27}N_3O_6$FeCl, 472.7 g/mol) C 45.73, H 5.76, N 8.89; Found C 45.35, H 5.28, N 9.22. ESI-MS spectrometry (positive mode, MeOH) $m/z = 419$ ($[L3\text{-Fe}]^+$, 100%); 455 ($[L3\text{-Fe-Cl}]^+$, 58%). IR (KBr, cm^{-1}): 3431 (m), 1679 (s, C═O), 1516 (s), 1455 (w), 1346 (m), 1329 (m), 1291 (s), 1280 (s), 1255 (m), 1092 (m), 1030 (m), 961 (s), 923 (s), 827 (s), 718 (w), 559 (w), 512 (w).

[L3-Fe-N_3] (23). This compound was synthesized by reaction of 1 equiv each of compound **22** and NaN_3 in MeOH. The reaction mixture was stirred for 3 h at room temperature, and an orange-reddish precipitate was observed, which was collected by filtration. Recrystallization of the above precipitate from MeCN in the dark led to the formation of orange crystals after 1 week. Yield: 50%. Anal. Calcd for the complex L3-Fe−N_3 ($C_{18}H_{25}N_6O_5$Fe, 461.3 g/mol) C 46.87, H 5.46, N 18.22; Found C 46.62, H 5.13, N 17.75. ESI-MS spectrometry (positive mode, MeOH) $m/z = 462$ ($[L3\text{-Fe-}N_3]^+$). IR (KBr, cm^{-1}): 3420 (m), 2064 (s, N_3), 1677 (s, C═O), 1514 (m), 1439 (m), 1338 (w), 1271 (m), 1252 (m), 1182 (m), 1086 (w), 1066 (w), 967 (w), 919 (w), 825 (m), 702 (w).

[L3-Fe-μ-O-Fe-L3]·6H_2O (24). This was synthesized in a similar way to **17**. Yield: 60%. Anal. Calcd for the complex L3-Fe-μ-O-Fe-L3·6H_2O ($C_{36}H_{62}N_6O_{17}Fe_2$, 962.6 g/mol): C 44.92, H 6.49, N 8.73; Found C 44.83, H 6.62, N 8.70. ESI-MS spectrometry (positive mode, MeOH) $m/z = 855$ ($[L3\text{-Fe-O-Fe-L3} + H]^+$). IR (KBr, cm^{-1}): 3440 (s), 1686 (s, C═O), 1619 (s, C═O), 1515 (s), 1356 (m), 1338 (m), 1292 (m), 1246 (m), 1184 (m), 1099 (m), 1090 (m), 1028 (m), 966 (m), 801 (s, Fe-O-Fe), 642 (w).

$^{57}FeCl_3$ was prepared according to the method reported in the literature[10] and isotopically enriched azido−Fe(III) complexes were prepared by using $^{57}FeCl_3$.

Physical Measurements. Infrared spectra (4000−400 cm^{-1}) of solid samples were recorded on a Perkin-Elmer 2000 FT-IR/FT-NIR Spectrometer as KBr disks. ESI-MS spectra were recorded on a Finnigan MAT 95 mass spectrometer. ^1H NMR spectra were measured on Bruker ARX 250 spectrometer. Cyclic voltammetry and coulometry were performed using an EG&G potentiostat/galvanostat model 273A with acetonitrile solutions of samples containing 0.10 M $[N(n\text{-}Bu)_4]PF_6$ as supporting electrolyte. Ferrocene was used as an internal standard, and all reported potentials are referenced versus the Fc^+/Fc couple. UV−vis spectra of solutions were measured on a Perkin-Elmer Lambda 19 spectrophotometer in the range 200−1000 nm. Temperature-dependent magnetic susceptibilities of powdered samples were measured using a SQUID magnetometer (Quantum Design) at 1.0 T (2.0−300 K). Corrections for underlying diamagnetism were made by using tabulated Pascal constants. X-band EPR spectra were recorded on a Bruker ESP 300E spectrometer equipped with a helium-flow cryostat (Oxford Instruments ESR 910). Mössbauer data were recorded on an alternating constant-acceleration spectrometer. The minimum experimental line width was 0.24 mm s^{-1} (full width at half-height). The field at the sample is oriented perpendicular to the γ-beam. The ^{57}Co/Rh source (1.8 GBq) was positioned at room temperature inside the gap of the magnet system at a zero-field position. Isomer shifts are quoted relative to iron metal at 300 K.

Spin Hamiltonian simulations of EPR spectra were performed with a program which was developed from the $S = 5/2$ routines of Gaffney and Silverstone[15] and which specifically makes use of the resonance-search procedure described therein.

X-ray Crystallographic Data Collection and Refinement of the Structures. Single crystals of **17**, **19**, and **20** and yellow crystals of **18** and **21** were coated with perfluoropolyether and picked up with looped nylon fibers. The crystals were immediately mounted in the nitrogen cold stream (100 K) of a Nonius Kappa-CCD diffractometer equipped with a Mo-target rotating-anode X-ray source and a graphite monochromator (Mo Kα, $\lambda = 0.71073$ Å). Final cell constants were obtained from least-squares fits of all measured reflections. Crystallographic data of the compounds are listed in Table 1. The Siemens ShelXTL[16] software package was used for solution and artwork of the structure; ShelXL97[17] was used for the refinement. The structures were readily solved by direct

(15) Gaffney, B. J.; Silverstone, H. J., In *Biological Magnetic Resonance*; Berliner, L. J., Reuben, J., Eds.; Plenum Press: New York, 1993; Vol. 13.

(16) *SHELXTL*, 5.0; Siemens Analytical X-Ray Instruments, Inc.: Madison, WI, 1994.

Table 1. Crystallographic Data of the Fe(III) Complexes Measured at 100 K

compounds	**17**	**18**	**19**	**20**	**21**
chem formula	$C_{35.5}H_{61}F_3Fe_2N_6Na_{0.5}O_{17.5}P_{0.5}$	$C_{18}H_{27}ClFeN_3O_5$	$C_{17}H_{23}FeN_6O_4$	$C_{13.5}H_{25}ClFeN_3O_{4.5}$	$C_{13}H_{23}FeN_6O_4$
fw	1047.59	456.73	431.26	392.67	383.22
cryst syst	monoclinic	triclinic	orthorhombic	monoclinic	orthorhombic
space group	$P2_1/n$	$P\bar{1}$	$P2_12_12_1$	$P2_1/c$	$Pbca$
a, Å	16.4915(6)	8.3266(6)	7.4733(2)	15.6291(6)	12.2611(6)
b, Å	16.5318(6)	13.0757(9)	12.9538(4)	6.9003(2)	15.8967(8)
c, Å	36.239(2)	19.190(1)	18.9587(4)	15.8036(6)	16.5101(9)
α, deg	90	73.25(1)	90	90	90
β, deg	97.229(5)	89.24(1)	90	103.783(5)	90
γ, deg	90	88.90(1)	90	90	90
V, Å^3	9801.5(7)	2000.39(2)	1835.35(8)	1655.3(1)	3218.0(3)
Z	8	4	4	4	8
ρ_{calcd}, g/cm	1.420	1.517	1.561	1.576	1.582
reflns collected/θ_{max}	125 003/26.00	40 720/31.01	46 198/30.99	24 975/31.03	47 895/28.49
no. of params/restr	1219/0	517/1	253/0	221/0	219/0
R1[a]; wR2 ($I > 2\sigma(I)$)[b]	0.0980; 0.2135	0.0412; 0.0927	0.0251; 0.0550	0.0262; 0.0611	0.0444; 0.0903
R[a] indices (all data)	0.1123; 0.2203	0.0503, 0.0970	0.0287, 0.0565	0.0331, 0.0640	0.0738, 0.1024

[a] $R1 = 3||F_o| - |F_c||/3|F_o|$. [b] $wR2 = [3[w(F_o^2 - F_c^2)^2]/3[w(F_o^2)^2]]^{1/2}$, $w = 1/\sigma^2(F_o^2) + (aP)^2 + bP$, where $P = [\max(0 \text{ or } F_o^2) + 2(F_c^2)]/3$.

and Patterson methods and subsequent difference Fourier techniques. All non-hydrogen atoms were refined anisotropically. Hydrogen atoms were placed at calculated positions and refined as riding atoms with isotropic displacement parameters, except for some hydrogen atoms in disordered solvent molecules.

The crystal structure of compound **17** is a disordered structure of low quality, but it confirms the atom connectivity and the discussed structural features without any doubt. The asymmetric unit in **17** contains two crystallographically independent complex molecules, a PF_6^- anion, a five-coordinate sodium cation, 14 water, and three methanol molecules. The five-coordinate sodium ion in a trigonal-bipyramidal environment is interesting but not unprecedented; there are several examples in the literature.[18] Disorder was found in the structure which might be due to a binding site competition between water and methanol molecules at the sodium cation. Four coordination sites are occupied by water molecules, but the fifth site binds water and methanol in a ~50:50 ratio. Therefore, the coordinating oxygen atom O(540) was refined with full occupation whereas the carbon atom C(541) was refined with a 50% occupation. The disorder continues throughout greater parts of the complicated hydrogen-bonding network of water and methanol molecules. Water molecule positions O(450), O(460), O(470), O(475), O(480), O(485), O(545), O(550), O(555), and methanol molecule O(490)−C(491) are affected and were refined with fractional occupation factors.

A water molecule of crystallization in **18** was found to be disordered over two sites. The split positions were refined with occupancies of 87% and 13% and restrained thermal displacement parameters using the EADP instruction of ShelXL. A methanol molecule in **20** was found to be disordered at a center of inversion. An occupation factor of 0.5 was therefore assigned to the O and C atoms.

Results and Discussion

Preparation of Ligands and Complexes. The synthetic routes employed are depicted in Scheme 1. Treatment of TACN with 2 equiv of BOC-ON leads to good yields and high purity of the *N*,*N*′-protected **1**,[14] from which R groups can be conveniently attached to the unprotected amine. Deprotection with CF_3CO_2H/CH_2Cl_2 followed by treatment with Et_3N or NaOH and then coupling with ethyl bromoacetate yields the ethyl diester of the desired ligands, which can be hydrolyzed with LiOH to produce the lithium salts **6**, **11**, and **16**.

Reaction of Li_2L (L = L1 and L3) with $[Fe(dmf)_6](ClO_4)_3$ in the presence of excess NaN_3 affords oxo-bridged di-iron species, whereas reaction with $FeCl_3$ yields the chloro species **18**, **20**, and **22**, which may be conveniently converted to the azido complexes **19**, **21**, and **23** by reaction with 1 equiv of NaN_3. Since NaN_3 may be hydrolyzed slowly in the presence of H_2O in the reaction mixture, it is recommended that 1−1.5 equiv of NaN_3 should be used in the formation of the corresponding azido compounds in order to prevent the formation of oxo-bridged dimeric species.

Crystal Structures. The structures of **17**−**21** at 100 K have been determined by single-crystal X-ray crystallography. Compound **17** crystallizes in $P2_1/n$ with $Z = 8$. The complex is neutral and contains a bridging oxo ligand that connects two pseudo-octahedrally coordinated Fe(III) ions. As shown in Figure 1, the bridging oxo-ligand is trans to one of the N atoms of the TACN ring. The average Fe−N and Fe−O bond lengths are 2.227(5) and 2.019(9) Å, respectively. The bridging oxo ligand is at an average distance of 1.791(9) Å from each Fe atom, and the Fe−O−Fe bond angle is 171.6(3)°. These parameters are typical for ferric μ-oxo dimers[19] and reflect π-bonding within the Fe−O−Fe core.[20]

Figures 2 and 3 show the structures of compounds **18**, **19**, **20**, and **21**. Table 1 summarizes the crystal data of the

(17) Sheldrick, G. M. *SHELXL-97. Program for Crystal Structure Refinement*; University of Göttingen: Göttingen, Germany, 1997.
(18) (a) Malkowsky, I. M.; Fröhlich, R.; Griesbach, U.; Pütter, H.; Waldvogel, S. R. *Eur. J. Inorg. Chem.* **2006**, 1690. (b) Hanna, T. A.; Liu, L. H.; Angeles-Boza, A. M.; Kou, X. D.; Gutsche, C. D.; Ejsmont, K.; Watson, W. H.; Zakharov, L. N.; Incarvito, C. D.; Rheingold, A. L. *J. Am. Chem. Soc.* **2003**, *125*, 6228. (c) Linti, G.; Coban, S.; Dutta, D. *Z. Anorg. Allg. Chem.* **2004**, *630*, 319. (d) Shen, L.; Jing, Z. M. *Acta Crystallogr. Sect. C-Cryst. Struct. Commun.* **2002**, *58*, M591.
(19) (a) Kurtz, D. M. *Chem. Rev.* **1990**, *90*, 585. (b) Roelfes, G.; Lubben, M.; Chen, K.; Ho, R. Y. N.; Meetsma, A.; Genseberger, S.; Hermant, R. M.; Hage, R.; Mandal, S. K.; Young, V. G.; Zang, Y.; Kooijman, H.; Spek, A. L.; Que, L.; Feringa, B. L. *Inorg. Chem.* **1999**, *38*, 1929. (c) Musie, G.; Lai, C. H.; Reibenspies, J. H.; Sumner, L. W.; Darensbourg, M. Y. *Inorg. Chem.* **1998**, *37*, 4086. (d) Berry, J. F.; Bill, E.; Garcia-Serres, R.; Neese, F.; Weyhermüller, T.; Wieghardt, K. *Inorg. Chem.* **2006**, *45*, 2027.
(20) Kappock, T. J.; Caradonna, J. P. *Chem. Rev.* **1996**, *96*, 2659.

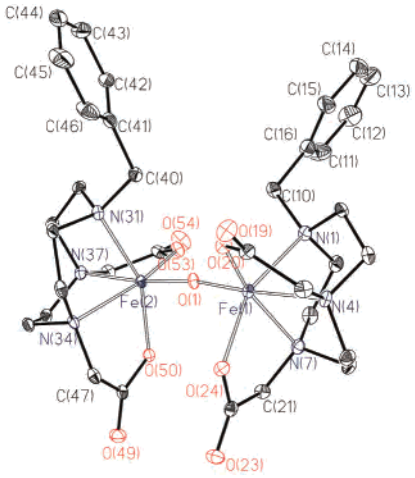

Figure 1. Thermal ellipsoid plot (30% probability) of **17** with atom-numbering scheme; hydrogen atoms, solvent molecules, and sodium salts in the asymmetric unit are omitted for clarity.

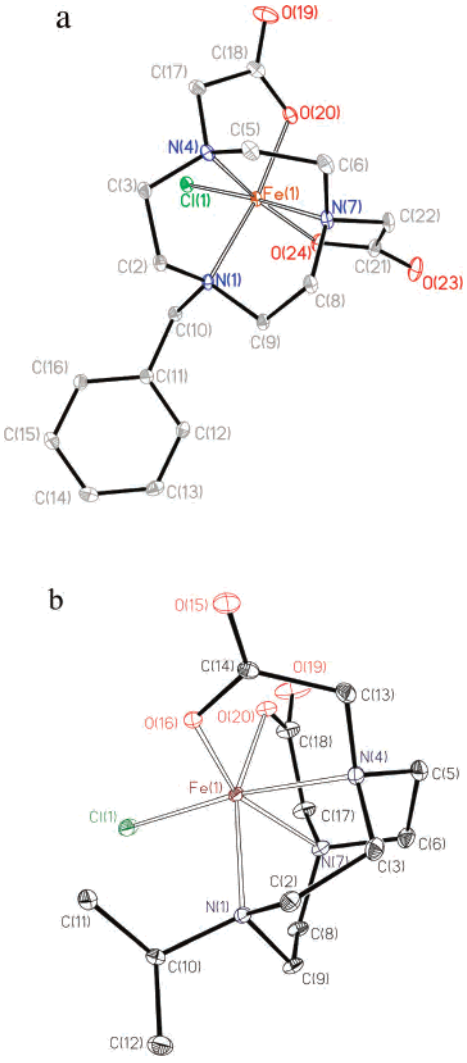

Figure 2. Thermal ellipsoid plots of (a) **18** and (b) **20** showing 30% probability displacement ellipsoids and the atom-numbering scheme; hydrogen atoms and solvent molecules are omitted for clarity.

Fe(III) complexes, and selected bond lengths are listed in Table 2. The crystal structures of the Fe(III)−chloro and Fe(III)−azido complexes appear to be similar except for the

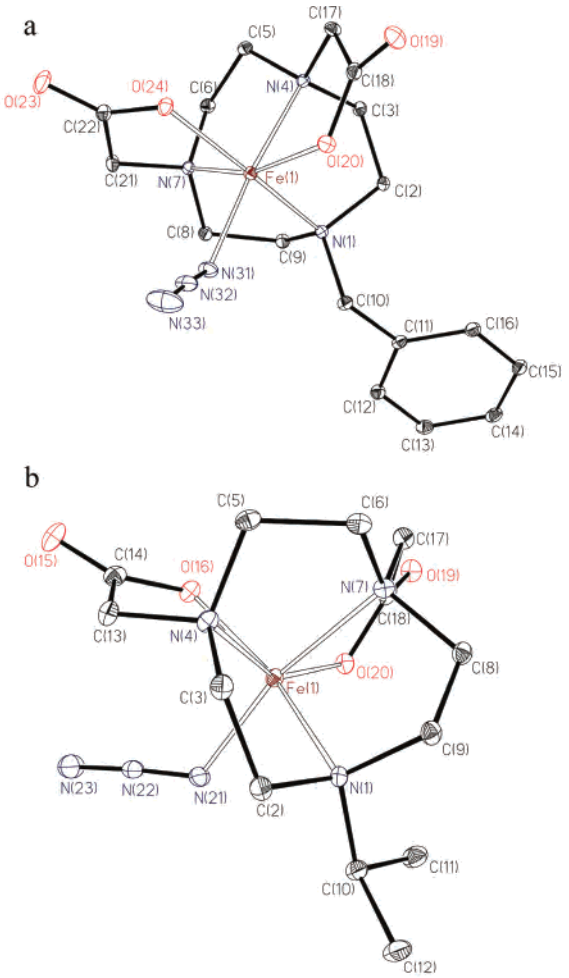

Figure 3. Perspective view (30% probability) and atom labels of (a) **19** and (b) **21**; hydrogen atoms and the solvent molecules are not shown here for clarity.

Table 2. Selected Bond Lengths (Å) of the Fe(III) Complexes

bond lengths (Å)	**17**	**18**	**19**	**20**	**21**
Fe(1)−O(1)	1.792(4)	–	–	1.9391(8)	2.001(2)
Fe(1)−O(20)	1.972(4)	1.975(1)	1.941(1)	1.9943(9)	1.952(2)
Fe(1)−O(24)	2.075(4)	1.945(1)	1.972(1)	–	–
Fe(1)−N(1)	2.237(5)	2.214(2)	2.211(1)	2.208(1)	2.237(2)
Fe(1)−N(4)	2.277(5)	2.166(2)	2.205(1)	2.214(1)	2.172(2)
Fe(1)−N(7)	2.168(5)	2.191(2)	2.161(1)	2.171(1)	2.196(2)
Fe(1)−Cl(1)	–	2.2762(5)	–	2.2831(3)	–
Fe(1)−N(21)	–	–	–	–	1.981(2)
Fe(1)−N(31)	–	–	1.975(1)	–	–
Fe(2)−O(1)	1.790(4)	–	–	–	–
Fe(2)−O(54)	1.986(4)	–	–	–	–
Fe(2)−O(50)	2.049(4)	–	–	–	–
Fe(2)−N(31)	2.223(5)	–	–	–	–
Fe(2)−N(34)	2.204(5)	–	–	–	–
Fe(2)−N(37)	2.255(5)	–	–	–	–

Cl^- and N_3^- anions. All the mononuclear Fe(III) complexes contain a pentadentate macrocycle with a 1,4,7-triazacyclononane-1,4-diacetato fragment. All these structures contain the ferric ion in an octahedral environment, which is slightly trigonally distorted, as evidenced by the N−Fe−O and N−Fe−X_{axial} angles larger than 100°. Each nitrogen atom of the macrocycle is unique in its coordination to the iron; therefore, the Fe−N(macrocycle) distances in **18**−**21** are all slightly different, though all are around 2.20 ± 0.03 Å. The

Fe−O distances are all likewise similar, averaging ∼1.97 Å, though the Fe−O bond *trans* to the N−R groups are uniformly longer by 0.03 Å when R = benzyl and 0.05 Å when R = isopropyl. The Fe−Cl bond lengths in **18** and **20** (∼2.28 Å) and the Fe−N_3 bond lengths in **19** and **21** (∼1.98 Å) are typical for Fe(III) chloro and azido complexes.

Magnetic and Spectroscopic Measurements. Oxo-bridged di-iron(III) complexes generally exhibit strong antiferromagnetic coupling of the two iron centers through the nearly linear μ-oxo unit.[19] Compounds **17** and **24** are no different; their measured effective magnetic moments at room temperature are 3.02 μ_B and 2.50 μ_B, respectively, values far less than the spin-only value for high-spin Fe(III) species ($S = 5/2$; $\mu_B = 5.92$). These values decrease monotonically to reach plateaus of less than 1 μ_B at low temperatures, indicating a diamagnetic ground state in each case. Fitting of these data using the spin Hamiltonian $H = -2J\,S1\cdot S2 + g\beta B\cdot S$ (where $S1 = S2 = 5/2$, J is the exchange coupling constant, g is the Landé factor, β is the Bohr magneton, and B is the magnetic field) yields isotropic J values of −80 and −113 cm^{-1} for **17** and **24**, respectively. The electronic g values in each case were set to 2, and the magnetic data were fitted taking into account paramagnetic impurities with $S = 5/2$ of 2.5% and 0.3% for **17** and **24**, respectively.

Magnetic susceptibility measurements of powdered samples of compounds **18**, **19**, **20**, **21**, **22**, and **23** show nearly temperature-independent magnetic moments of 5.85 μ_B, 5.80 μ_B, 5.83 μ_B, 5.78 μ_B, 5.80 μ_B, and 5.76 μ_B at 290 K, respectively, which are clearly indicative of five unpaired electrons and are in good agreement with the spin-only value of 5.92 μ_B for octahedral high-spin Fe(III) ions. Further investigation of the azido−Fe(III) complexes with various temperatures (4.2−300 K) and various field strengths (1, 4, and 7 T; VTVH data) allows the determination of zero-field splitting parameters. The observed curves of $M_{mol}/Ng\beta$ vs $H\beta/kT$ for the azido−Fe(III) complexes can be well fit with the spin Hamiltonian in eq 1:

$$H = g\beta\vec{B}\vec{S} + D\left[\vec{S}_z^2 - \frac{1}{3}S(S+1) + E/D(\vec{S}_x^2 - \vec{S}_y^2)\right] \quad (1)$$

In which D represents the axial zero-field splitting parameter and E/D parametrizes the rhombicity of the zero-field splitting tensor. Fitting of the VTVH data (see Figure S1) with $S = 5/2$ yields $g = 2.0$ (fixed), $E/D = 0.33$ for all three complexes; $D = 0.48$ cm^{-1}, $\theta = -0.61$ K for **19**; $D = 0.48$ cm^{-1}, $\theta = -0.85$ K for **21** and $D = 0.44$ cm^{-1}, $\theta = -0.50$ K for **23**. All these parameters are in line with the d^5 electron configuration of the high-spin Fe(III) ions in their trigonally distorted environment.

The X-band EPR spectra of compounds **18**−**23** recorded in normal (perpendicular) mode at 4 K display rhombic spectra with a broad signal at $g = 4.28$ typical of an octahedral high-spin iron(III) ion. The EPR spectra of the azido−Fe(III) complexes were successfully simulated using the effective g value formalism for the zero-field split Kramers doublets of a rhombic $S = 5/2$ system with $E/D = 0.33$ and $D = 0.5 \pm 0.2$ cm^{-1} (the D values were determined by the susceptibility measurement above). The D value here is far below the typical range 3−15 cm^{-1} found for that of high-spin Fe(III) ions in porphyrins,[21] as expected for non-heme species with lesser tetragonal distortion.[22,23] As the zero-field splitting of the $^6A_1$ ground state in a simplistic picture[24] is due to spin−orbit coupling with the first excited quartet term $^4A_2$, the low D value and the correspondingly large $^6A_1/^4A_2$ reflect a smaller $10Dq$ splitting of the e_g and t_{2g} levels in the TACN-derived complexes as compared to iron−porphyrin complexes.

Table 3. Zero-Field Mössbauer Parameters for Fe(III) Complexes with L1, L2, and L3 at 80 K

compounds	δ, mm/s	ΔE_Q, mm/s
17	0.44	1.52
18	0.41	0.58
19	0.46	0.61
21	0.46	0.82
23	0.56	0.47
24	0.45	1.52

Table 4. Electronic Spectra of Azido−Fe(III) Complexes in CH_3CN Solution

complexes	λ_{max}, nm (ϵ, L/mol·cm)[a]
19	250 (1.3×10^4), 315 (sh), 420 (4.4×10^3)
21	250 (5.3×10^3), 310 (sh), 435 (1.9×10^3)
23	246 (9.6×10^3), 315 (sh), 419 (3.3×10^3).

[a] sh = shoulder

Table 3 lists the results of zero-field Mössbauer measurements of the Fe(III) complexes. The isomer shifts of these complexes are in the range of 0.45−0.56 mm/s, typical for high-spin octahedral Fe(III) complexes.[10] The quadrupole splittings for the mononuclear complexes are small and between 0.47 and 0.72 mm/s, reflecting the high symmetry of the high-spin d^5 electron configuration. For the μ-oxo dimers, the quadrupole splittings are around 1.5 mm/s, which are in the normal range for μ-oxo-bridged dinuclear Fe(III) compounds.[25]

UV−vis spectra of the azido−Fe(III) complexes have been measured in MeCN solution at room temperature, and Table 4 summarizes the data. The spectra contain azide-to-Fe charge-transfer bands in the range of 419−435 nm which are so assigned due to their absence in the corresponding chloro complexes. Similar assignments have been made in the case of azido Fe(cyclam) complexes.[10]

Electrochemistry. The electrochemistry of the azido−Fe(III) complexes **19**, **21**, and **23** in MeCN has been studied by cyclic and square-wave voltammetry. Table 5 summarizes the redox potentials of the compounds, which are referenced versus the ferrocene/ferrocenium couple. The chloro complexes were also studied, but only irreversible waves were observed.

(21) Debrunner, P. G. In *Iron Porphyrins*; Lever, A. B. P., Gray, H. B., Eds.; VCH: Weinheim, 1989; Vol. 3, p 137.
(22) Boča, R. *Coord. Chem. Rev.* **2004**, *248*, 757.
(23) Berry, J. F.; Bill, E.; Bothe, E.; Neese, F.; Wieghardt, K. *J. Am. Chem. Soc.* **2006**, *128*, 13515.
(24) (a) Maltempo, M. M. *J. Chem. Phys.* **1974**, *61*, 2540. (b) Maltempo, M. M.; Moss, T. H. *Q. Rev. Biophys.* **1976**, *9*, 181.
(25) Jüstel, T.; Muller, M.; Weyhermüller, T.; Kressl, C.; Bill, E.; Hildebrandt, P.; Lengen, M.; Grodzicki, M.; Trautwein, A. X.; Nuber, B.; Wieghardt, K. *Chem.-Eur. J.* **1999**, *5*, 793.

Table 5. Redox Potentials of Azido−Fe(III) Complexes

complexes	E, V vs Fc^+/Fc[a]
19	−749 mV r, 1112 mV r
21	−738 mV r, 1157 mV[b]
23	−734 mV r, 1116 mV[b]

[a] For reversible (r), one-electron processes $E_{1/2}$ is given ($E_{1/2} = E_{p,ox} + E_{p,red}$)/2. [b] The redox potentials of the quasi-reversible peak at −20 °C have been given. All other measurements have been done at room temperature. Solvents: MeCN; supporting electrolyte: 0.10 M $[N(n\text{-}Bu)_4]PF_6$.

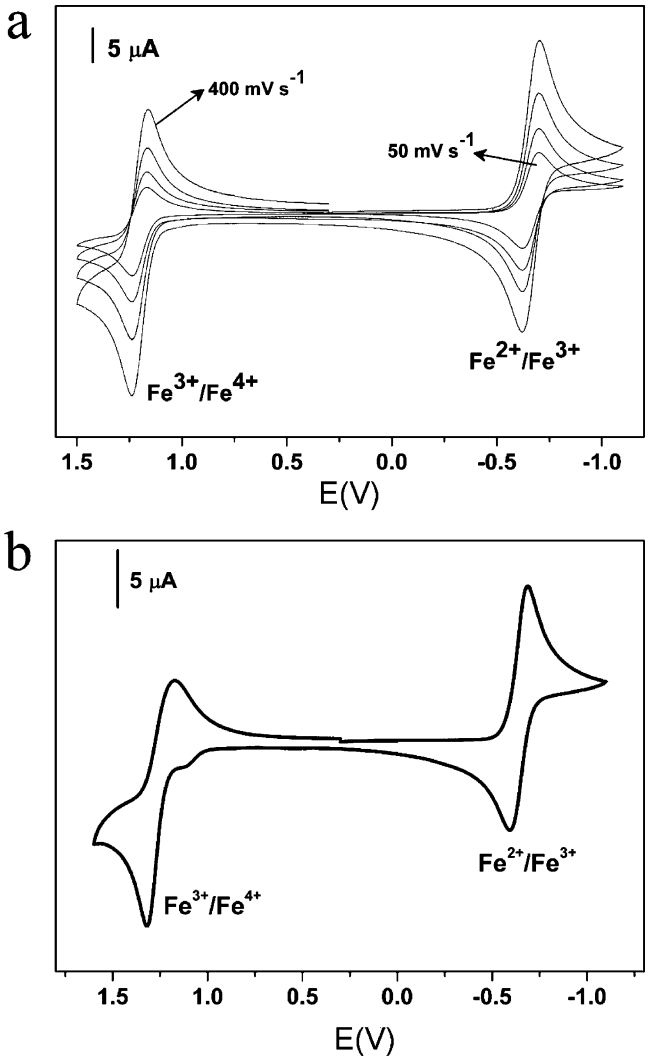

Figure 4. Cyclic voltammogram of (a) **19** (1 mM) in MeCN at room temperature (25 °C, 0.10 M $[N(n\text{-}Bu)_4]PF_6$ supporting electrolyte; glassy carbon working electrode; scan rates 0.05, 0.10, 0.20, 0.40 V/s). (b) **21** in CH_3CN solution (0.10 M $[N(n\text{-}Bu)_4]PF_6$, recorded at a scan rate of 0.20 V/s at a glassy carbon electrode at −20 °C. The small irreversible peak at +1.1 V corresponds to an impurity of the chloro complex.

All three azido complexes show two important electrochemical processes: a one-electron reduction between −734 and −749 mV and a one-electron oxidation process above 1100 mV which is fully reversible for **19**, but less so for the other two complexes (see Figure 4). The second process is irreversible for **21** and **23** at room temperature, most likely due to an E−C process, but when measured at −20 °C, these waves become quasi-reversible, indicating a greater stability of the oxidized forms at lower temperatures. Since the pentadentate ligands used in this study contain the redox-stable 1,4,7-triazacyclononane-1,4-diacetate backbone,[14] the redox processes can be safely assigned to the metal center.

Three electron-transfer series involving six-coordinate Fe(II), Fe(III), and Fe(IV) complexes have been recently reported, all based on the macrocyclic ligand 1,4,8-trimethyl-1,4,8,11-tetraazacyclotetradecane-11-acetate (Me_3cyclam-acetate) which enforces a compressed octahedral geometry in the complexes.[23,26] Here, a corresponding series of trigonally distorted complexes, comprised of **19** and its reduction product (**19red**) and oxidation product (**19ox**) is presented. A spectroscopic study of this series is presented so that the highly oxidized complex **19ox** may be considered in the context of the growing number of Fe(IV) complexes which have recently been reported.[23,26−29]

The reduction potential of **19** (−749 mV) is the same as the low-spin azido complex $[(\text{cyclam-acetate})FeN_3]^+$,[11] despite the difference in spin state and the charge difference of the two complexes. Most likely, these two effects fortuitously cancel each other in this case. Likewise, the oxidation potential of **19** is very close to that of $[(Me_3\text{cyclam-acetate})FeN_3]^+$.[26] Thus, **19** has a large potential range in which the Fe(III) species is stable.

Combined UV−vis/electrochemistry measurements of **19** were performed at −20 °C by use of an optically transparent thin-layer electrochemical cell (OTTLE cell). The electronic spectra of oxidized and reduced species of **19** are shown in Figure 5 (**21** was also studied, and its spectra are given in the Supporting Information as Figure S2). Upon reduction, solutions of **19** bleach as the absorptions at 250, 315, and 420 nm all lose intensity. Upon oxidation, however, the solution becomes more colored as all three bands undergo a bathochromic shift and a new band is observed at 780 nm indicative of the Fe(IV) species **19ox**. Similar long-wavelength bands have been observed in the previously studied $[(Me_3\text{cyclam-acetate})Fe^{IV}N_3]^{2+}$ species,[26] as well as in Fe(IV)−oxo species for which they have been assigned as d−d transitions.[30]

Oxidation and reduction of **19** (and **21**; see Figure S3) were also monitored by IR spectroscopy since two intense absorption bands at ∼2066 and ∼1674 cm^{-1} corresponding to the azide stretch and the C═O stretch of the pendent acetate groups appear in a region where the solvent and

(26) Berry, J. F.; Bill, E.; Bothe, E.; Weyhermüller, T.; Wieghardt, K. *J. Am. Chem. Soc.* **2005**, *127*, 11550.
(27) (a) Slep, L. D.; Mijovilovich, A.; Meyer-Klaucke, W.; Weyhermüller, T.; Bill, E.; Bothe, E.; Neese, F.; Wieghardt, K. *J. Am. Chem. Soc.* **2003**, *125*, 15554. (b) Costas, M.; Rohde, J. U.; Stubna, A.; Ho, R. Y. N.; Quaroni, L.; Münck, E.; Que, L. *J. Am. Chem. Soc.* **2001**, *123*, 12931. (c) Zheng, H.; Yoo, S. J.; Münck, E.; Que, L. *J. Am. Chem. Soc.* **2000**, *122*, 3789. (d) Dong, Y. H.; Que, L.; Kauffmann, K.; Münck, E. *J. Am. Chem. Soc.* **1995**, *117*, 11377. (e) Kostka, K. L.; Fox, B. G.; Hendrich, M. P.; Collins, T. J.; Rickard, C. E. F.; Wright, L. J.; Münck, E. *J. Am. Chem. Soc.* **1993**, *115*, 6746. (f) Rohde, J. U.; In, J. H.; Lim, M. H.; Brennessel, W. W.; Bukowski, M. R.; Stubna, A.; Münck, E.; Nam, W.; Que, L. *Science* **2003**, *299*, 1037.
(28) Collins, T. J.; Kostka, K. L.; Münck, E.; Uffelman, E. S. *J. Am. Chem. Soc.* **1990**, *112*, 5637.
(29) Lim, M. H.; Rohde, J. U.; Stubna, A.; Bukowski, M. R.; Costas, M.; Ho, R. Y. N.; Münck, E.; Nam, W.; Que, L. *Proc. Natl. Acad. Sci. U.S.A.* **2003**, *100*, 3665.
(30) Decker, A.; Rohde, J. U.; Que, L.; Solomon, E. I. *J. Am. Chem. Soc.* **2004**, *126*, 5378.

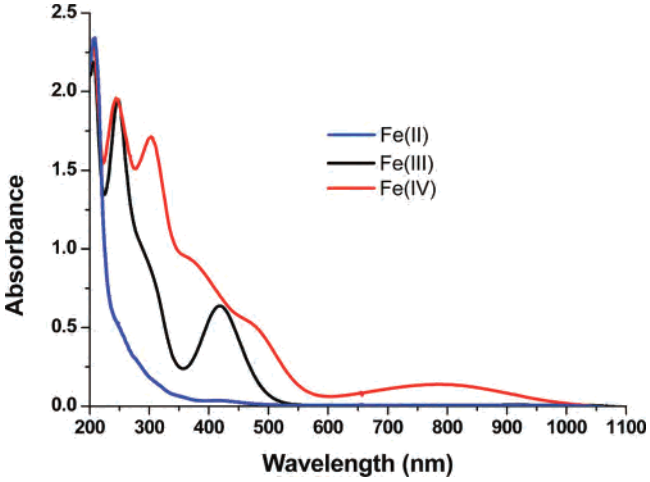

Figure 5. UV−vis spectra of **19red**, **19**, and **19ox** (2.7×10^{-4} mol/L) in MeCN at −20 °C (see Supporting Information for **21**).

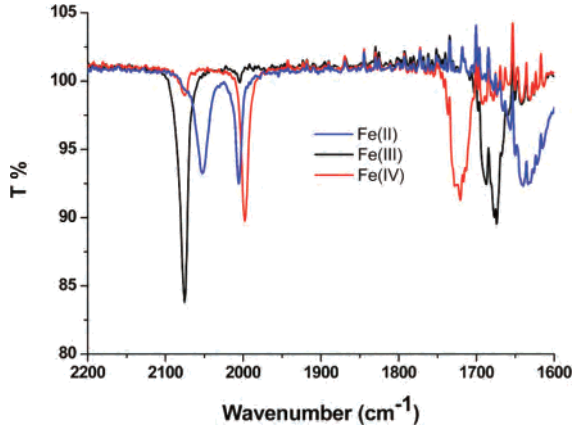

Figure 6. IR spectral change observed during electro-oxidation and electro-reduction of **19** (1 mM) in MeCN at −20 °C.

electrolyte do not absorb. Both of these bands exhibit significant changes upon oxidation and reduction and the spectra (Figure 6) show almost 90%∼100% recovery of the starting material on re-oxidation of **19red** or re-reduction of **19ox**, indicating that no ligands are removed during the coulometry.

During the one electron reduction process of **19**, both the azide stretch and the C═O stretch of the pendent acetate groups decrease dramatically as new bands at 2055, 2005, and 1635 cm^{-1} appear and increase. The C═O stretch shifts to lower energy as the oxidation state of the metal is decreased, suggesting a weaker Fe−O bond with decreased oxidation state, as has been quantified previously.[23,31] There are two new azide bands at around 2000 cm^{-1}, which may be due to the presence of two different orientations of the azido ligand (the Fe−N−N linkage is bent, and therefore the azido group has four different directions in which it may be bent over the ligand).

For the one-electron oxidation process, the C═O stretch moves to higher energy (1722 cm^{-1}) while the azide stretch moves to lower frequency (1996 cm^{-1}). In both cases, the azide stretch shifts to lower energy, emphasizing greater π

(31) Berry, J. F.; Bill, E.; Bothe, E.; George, S. D.; Mienert, B.; Neese, F.; Wieghardt, K. *Science* **2006**, *312*, 1937.

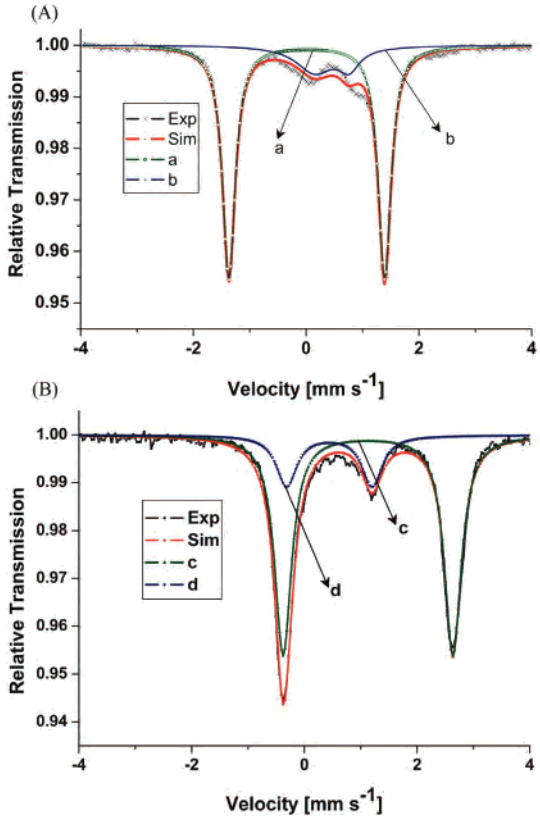

Figure 7. Zero-field Mössbauer spectra measured at 80 K of (A) electro-oxidation at −40 °C and (B) electro-reduction at −20 °C of **19** (1 mM) in CH_3CN. (a) **19ox**, (b) **19**, (c) **19red**, (d) **17**.

donation of azide to Fe(IV) and Fe(II) relative to the high-spin Fe(III) ion. The C═O and azide stretches are affected significantly and characteristically with the different oxidation states of iron as +2, +3, and +4, as has been previously shown for the analogous Me_3cyclam-acetate complexes.[26] Similar IR profiles have been observed during electro-oxidation and reduction of **21** (see Figure S3).

Electrochemically generated solutions of ^{57}Fe isotopically enriched samples of the oxidation and reduction products of **19** were also examined by Mössbauer spectroscopy in order to provide further support of the Fe(IV) assignment in **19ox** and determine the spin states of the new Fe(II) and Fe(IV) species.

In **19red**, the Mössbauer spectrum (Figure 7B) shows a strong signal (species **c**) with quadrupole splitting ΔE_Q = 3.013 mm/s and isomer shift δ = 1.13 mm/s, which allows unambiguous assignment as a high-spin Fe(II) species which accounts for 78% of the spectral intensity. The Mössbauer parameters of **19red** are comparable to those of similar high-spin Fe(II) compounds found in literature.[10,26] The remaining 22% of intensity (species **d**) is fitted to the L1-Fe(III)-O-Fe(III)-L1 species (δ = 0.44 mm/s, ΔE_Q = 1.52 mm/s), most likely formed via aerial oxidation of the sample.

The Fe(IV) species was electrochemically generated at −40 °C in MeCN and coulometry was stopped when a charge corresponding to 95% of 1 F/mol was passed. Here, the main feature of the Mössbauer spectrum (Figure 7A) is a doublet (species **a**) with large ΔE_Q of 2.76 mm/s and a low δ value of 0.01 mm/s, which accounts for 81% of the

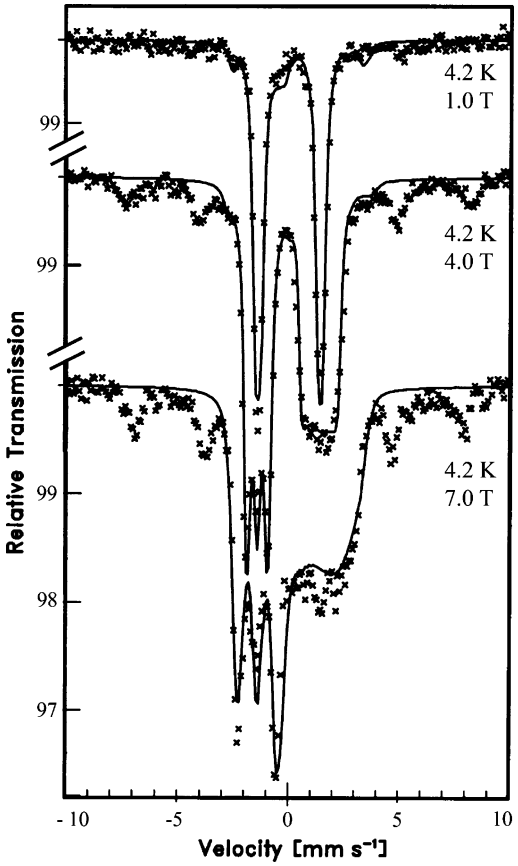

Figure 8. Mössbauer spectra of **19ox** measured in applied magnetic fields (perpendicular to the γ source) of 1.0, 4.0, and 7.0 T all at 4.2 K. These were simulated assuming fast spin relaxation with a spin Hamiltonian analysis with the following parameters: $S = 2$, $\delta = 0.01$, $\Delta E_Q = 2.77$, $D = 6.68$ cm^{-1}, $E/D = 0$, $A_{xx} = -3.1$ T, $A_{yy} = -0.3$ T, $A_{zz} = +12.8$ T. Due to the presence of remaining high-spin Fe(III) impurities and the large axial zero-field splitting value, this fit is not unique as described in the text.

spectral intensity and is more than 0.3 mm/s lower than that of **19** itself, which indicates that **19ox** is a genuine Fe(IV)−azido complex. The δ value is also comparable to those found in Fe(IV)−oxo compounds,[11,29] though higher than in the five-coordinate Fe(IV) species [Fe^{IV}(MAC*)Cl]$^-$ ($\delta = -0.03$ mm/s, MAC* is a macrocyclic tetra-anionic ligand[28]). The ΔE_Q value of 2.76 mm/s is larger than those reported with either low-spin ferryl species ($S = 1$)[11,29] or high-spin five-coordinate species ($S = 2$).[28] Similar ΔE_Q values have, however, been observed for low-spin non-oxo Me$_3$cyclam-acetate Fe(IV) species having axial chloro or fluoro ligands.[23]

Mössbauer spectra of **19ox** were measured at 4.2 K in applied magnetic fields of 1, 4, and 7 T (Figure 8). The spectra show very little magnetic splitting, in accord with a large axial zero-field splitting. Unfortunately, since the splitting is so small, the magnetically perturbed spectra may be fit in a number of different ways.[32] Reasonable fits include a high-spin model ($S = 2$) having $D = 6.7$ cm^{-1}, and $A = \{-3.1, -0.3, +12.8\}$ T, although this fit is no better than low spin ($S = 1$) fits with $D \approx 6-7$ cm^{-1} and $A = \{-1$ to $-2, -9$ to $-11, +13$ to $+17\}$ T. Thus, the spin state cannot be determined at this time.

(32) Fitting of these spectra is also complicated by the residual high-spin Fe(III) species.

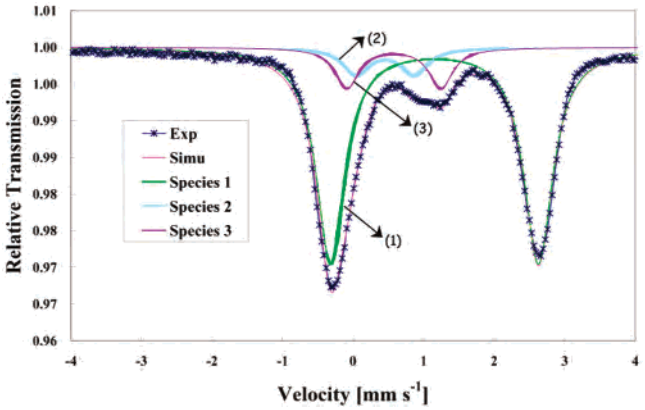

Figure 9. Mössbauer spectrum of **21** after photolysis at room temperature in MeCN (irradiation wavelength: 330 nm). The spectra were fit with three components: species (1) is a high-spin Fe(II) species; species (2) is **21**, and species (3) is L2−^{57}Fe−O−^{57}Fe−L2.

Photolysis of 21. Photolysis of a 10 mM solution of **21** in dry acetonitrile was performed at room temperature with a Rayonet Photochemical Reactor (RPR-100) equipped with 480, 419, or 330 nm tubes. Since the photolysis products of azido−manganese complexes have been shown to be wavelength-dependent,[33] we decided to examine the photochemistry of **21** using both visible (480, 419 nm) and UV (330 nm) light. The photolysis process was followed optically by changes in the color of the species from orange to pale beige and monitored by IR spectroscopy and Mössbauer spectroscopy.

When the photolysis was carried out in air at 330 nm at 298 K for 4 h, the solution is bleached, and IR spectra show that the azide stretch gradually loses intensity. The zero-field Mössbauer spectrum (80 K, Figure 9) of the product solution shows an intense quadrupole doublet, species 1, with $\delta = 1.15$ mm/s and $\Delta E_Q = 2.95$ mm/s, which accounts for 79% of the spectral intensity. The isomer shift and quadrupole splitting parameters clearly indicate that species 1 is a high-spin Fe(II) complex resulting from the photoreduction of the starting material. Unreacted **21** is also present at 9% relative intensity, species 2 ($\delta = 0.46$ mm/s and $\Delta E_Q = 0.82$ mm/s). The remaining 12% of the intensity is fit with parameters similar to those of L2-^{57}Fe-O-^{57}Fe-L2 (species 3, $\delta = 0.58$ mm/s and $\Delta E_Q = 1.33$ mm/s), most likely the result of oxidation of species 1 by air. Irradiation at 419 and 480 nm gave similar results.

Although photolysis of **21** in liquid solution proceeds almost completely via photoreduction, its photochemistry was further investigated in frozen solution in an attempt to promote photo-oxidation. Photolysis temperature has been found to be a very critical experimental parameter governing the product distribution.[10] To date, Fe(V) nitrido species have only been observed during low-temperature photolysis.[10,11]

Samples for photolysis at 77 K were prepared via the previously described method II.[10] Photolysis was performed on a stirred suspension of a fine snow of **21** in acetonitrile kept in liquid nitrogen with stirring with 419 nm irradiation

(33) Meyer, K.; Bendix, J.; Metzler-Nolte, N.; Weyhermüller, T.; Wieghardt, K. *J. Am. Chem. Soc.* **1998**, *120*, 7260.

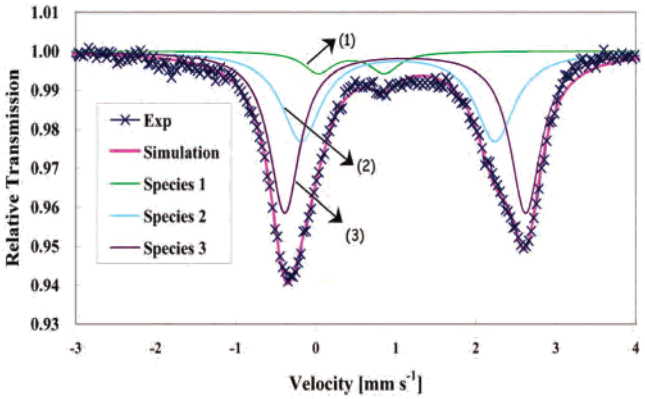

Figure 10. Mössbauer spectrum (80 K) of photolysis of **21** at 77 K in MeCN for 4 h (irradiation wavelength: 330 nm). The fit (solid line) is comprised of unreacted **21** (species 1) and two high-spin Fe(II) species 2 and species 3 with large quadrupole splitting.

in a Rayonet reactor. After photolysis of the azide complex for 4 h, the color of the snow faded from orange to white. A portion of the photolyzed snow was packed in a Mössbauer cup for analysis.

The features of the resulting zero-field Mössbauer spectrum (Figure 10) are two intense quadrupole doublets, species 2 with $\delta = 1.02$ mm/s, $\Delta E_Q = 2.43$ mm/s and species 3 with $\delta = 1.11$ mm/s and $\Delta E_Q = 2.99$ mm/s, respectively, which account for almost 70% of the spectral intensity. These isomer shifts and quadrupole splitting parameters can be assigned to two high-spin Fe(II) species, and species 3 is very similar to the photoreduction product from the liquid solution measurement. We suggest therefore that species 3 has MeCN occupying the sixth coordination site, whereas species 2 may be five-coordinate. The remaining 30% of the intensity was fit with parameters of the starting material. Again, irradiation at 330 and 480 nm gave similar results.

It is our observation that photolysis of high-spin Fe(III)−azido complexes generally yields photoreduced products, whereas photo-oxidation to Fe(V)−nitrido species has only been directly observed upon photolysis of low-spin precursors. This observation is supported by the data presented in this paper, as well as in previously reported systems.[10−12,25,31] The most poignant examples are from studies of ferric azido complexes with supporting cyclam-based ligands. For example, the complexes *cis*- and *trans*-$[(\text{cyclam})\text{Fe}(N_3)_2]^+$ were both subjected to photolysis. Whereas photolysis of the trans isomer, which is low spin, led to the observation of a species formulated as *trans*-$[(\text{cyclam})\text{FeN}(N_3)]^+$ containing the Fe(V) ion, no such species was observed in the case of the *cis* isomer, which is high spin.[10]

A simple four-state model is proposed to account for the different reactivity as a function of the spin state of the iron (see Chart 1).

The four states involved are shown as four different potential energy curves in Chart 1: (1) low-spin $LFeN_3$ (purple curve), (2) high-spin $LFeN_3$ (orange curve), (3) $LFe^{V}{\equiv}N + N_2$ (red curve), and (4) $LFe^{II} + N_3^{\bullet}$ (blue curve). The minima of these curves are offset in the direction of the abscissa by their estimated average Fe−ligand bond distances. In this regard, the pair of states involving low-spin

Chart 1

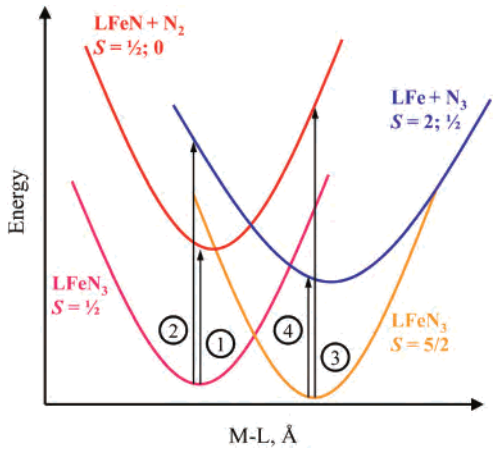

Scheme 2

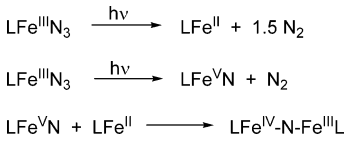

Scheme 3

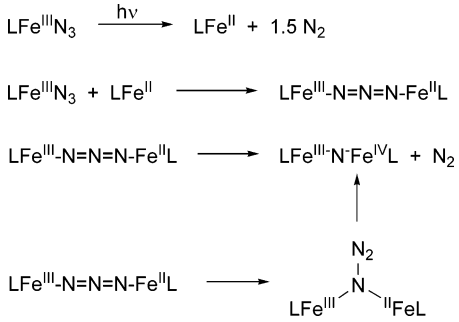

FeN_3 and $LFe^{V}{\equiv}N$ are not expected to be very different from one another[12] and neither are high-spin $LFeN_3$ and LFe^{II}.[23] The energies of these states are also estimated in Chart 1, and four Frank−Condon transitions are drawn between these states: (1) and (3) correspond to photo-oxidation processes, and (2) and (4) are photoreductions. It is clear that the processes most kinetically favored will be those for which the reorganization energy is minimized, i.e., processes (1) and (4). Importantly, these are also processes for which the total spin of the system is conserved, a specific requirement for photochemical reactions since photons carry no angular momentum. Thus, photo-oxidation is favored from a low-spin Fe(III) precursor and photoreduction is favored when the Fe(III) precursor is high-spin.

It is important to clarify this last statement in view of dinuclear Fe(IV)−N−Fe(III) complexes which are known to form during photolysis of high-spin ferric azido complexes.[10,25] It is often presumed that these species form via the reaction sequence given in Scheme 2, implying the intermediacy of an $Fe^{V}{\equiv}N$ species.

Given that the central reaction in this sequence is likely disfavored, the formation of these mixed-valent $Fe^{III/IV}$ species may involve reactions given in Scheme 3, which feature a μ-azido di-Fe(II/III) intermediate.

Conclusions

To summarize, three new redox-innocent pentadentate ligands containing the 1,4,7-triazacyclononane-1,4-diacetate motif have been synthesized and their coordination chemistry with Fe(III) has been studied. Eight new Fe(III) complexes have been synthesized with these ligands. X-ray structures of five Fe(III) complexes reveal that three nitrogen atoms in the TACN backbone coordinate facially to Fe(III) ions with two additional coordination sites occupied by two pendent acetate groups and a chloride or azide anion or a bridging oxygen atom as the sixth ligand. Characterization of the iron complexes by magnetic susceptibility measurements and zero-field Mössbauer measurements are in good agreement with the high-spin state of the Fe(III) ions. EPR spectra of the azido−Fe(III) complexes have effective g values around 4.3, which can be well fit with $E/D = 0.33$ and $D = 0.46 \pm 0.2$ cm^{-1}. The zero-field splitting parameters agree well with those obtained by VTVH magnetic susceptibility measurements and indicate a small $10Dq$ splitting between the e_g and t_{2g} levels. Spectroelectrochemistry of **19** has shown that the corresponding Fe(IV) species **19ox** can be generated coulometrically at −40 °C. Compounds **19**, **19red**, and **19ox** show very characteristic IR and UV−vis profiles. It should be noted that **19ox** represents a potential precursor to a new Fe(VI)−nitrido complex,[31] a property we plan to pursue. Photolysis of **21** at room temperature with different wavelengths such as 480, 419, and 330 nm shows that the formation of high-spin Fe(II) species or sometimes Fe(III)−O−Fe(III) dinuclear compounds, but photolysis performed at 77 K shows two types of high-spin Fe(II) species, which are likely five- and six-coordinate compounds, respectively. A simple four-state model has been put forth to explain the observation that high-spin Fe(III) azido complexes undergo primarily photoreduction.

Acknowledgment. We are grateful to the Fonds der Chemischen Industrie for financial support. J.F.B. thanks the Alexander von Humboldt Stiftung for support in the form of a postdoctoral fellowship.

Supporting Information Available: Figures S1, S2, and S3, as well as X-ray crystallographic information in CIF format. This material is available free of charge via the Internet at http://pubs.acs.org.

IC062001J